EUROPEAN LABORATORY FOR PARTICLE PHYSICS

Search for B_s^0 oscillations using inclusive lepton events

The ALEPH Collaboration [1]

Abstract

A search for B_s^0 oscillations is performed using a sample of semileptonic b-hadron decays collected by the ALEPH experiment during 1991–1995. Compared to previous inclusive lepton analyses, the proper time resolution and b-flavour mistag rate are significantly improved. Additional sensitivity to B_s^0 mixing is obtained by identifying subsamples of events having a B_s^0 purity which is higher than the average for the whole data sample. Unbinned maximum likelihood amplitude fits are performed to derive a lower limit of $\Delta m_s > 9.5$ ps^{-1} at 95% CL. Combining with the ALEPH D_s^- based analyses yields $\Delta m_s > 9.6$ ps^{-1} at 95% CL.

---

[1]See the following pages for the list of authors.

The ALEPH Collaboration

R. Barate, D. Buskulic, D. Decamp, P. Ghez, C. Goy, J.-P. Lees, A. Lucotte, E. Merle, M.-N. Minard, J.-Y. Nief, B. Pietrzyk

Laboratoire de Physique des Particules (LAPP), IN²P³-CNRS, F-74019 Annecy-le-Vieux Cedex, France

R. Alemany, G. Boix, M.P. Casado, M. Chmeissani, J.M. Crespo, M. Delfino, E. Fernandez, M. Fernandez-Bosman, Ll. Garrido,[15] E. Graugès, A. Juste, M. Martinez, G. Merino, R. Miquel, Ll.M. Mir, I.C. Park, A. Pascual, I. Riu, F. Sanchez

Institut de Física d'Altes Energies, Universitat Autònoma de Barcelona, E-08193 Bellaterra (Barcelona), Spain[7]

A. Colaleo, D. Creanza, M. de Palma, G. Gelao, G. Iaselli, G. Maggi, M. Maggi, S. Nuzzo, A. Ranieri, G. Raso, F. Ruggieri, G. Selvaggi, L. Silvestris, P. Tempesta, A. Tricomi,[3] G. Zito

Dipartimento di Fisica, INFN Sezione di Bari, I-70126 Bari, Italy

X. Huang, J. Lin, Q. Ouyang, T. Wang, Y. Xie, R. Xu, S. Xue, J. Zhang, L. Zhang, W. Zhao

Institute of High-Energy Physics, Academia Sinica, Beijing, The People's Republic of China[8]

D. Abbaneo, U. Becker, P. Bright-Thomas,[24] D. Casper, M. Cattaneo, F. Cerutti, V. Ciulli, G. Dissertori, H. Drevermann, R.W. Forty, M. Frank, R. Hagelberg, A.W. Halley, J.B. Hansen, J. Harvey, P. Janot, B. Jost, I. Lehraus, P. Mato, A. Minten, L. Moneta,[21] A. Pacheco, F. Ranjard, L. Rolandi, D. Rousseau, D. Schlatter, M. Schmitt,[20] O. Schneider, W. Tejessy, F. Teubert, I.R. Tomalin, H. Wachsmuth

European Laboratory for Particle Physics (CERN), CH-1211 Geneva 23, Switzerland

Z. Ajaltouni, F. Badaud, G. Chazelle, O. Deschamps, A. Falvard, C. Ferdi, P. Gay, C. Guicheney, P. Henrard, J. Jousset, B. Michel, S. Monteil, J-C. Montret, D. Pallin, P. Perret, F. Podlyski, J. Proriol, P. Rosnet

Laboratoire de Physique Corpusculaire, Université Blaise Pascal, IN²P³-CNRS, Clermont-Ferrand, F-63177 Aubière, France

J.D. Hansen, J.R. Hansen, P.H. Hansen, B.S. Nilsson, B. Rensch, A. Wäänänen

Niels Bohr Institute, DK-2100 Copenhagen, Denmark[9]

G. Daskalakis, A. Kyriakis, C. Markou, E. Simopoulou, I. Siotis, A. Vayaki

Nuclear Research Center Demokritos (NRCD), GR-15310 Attiki, Greece

A. Blondel, G. Bonneaud, J.-C. Brient, P. Bourdon, A. Rougé, M. Rumpf, A. Valassi,[6] M. Verderi, H. Videau

Laboratoire de Physique Nucléaire et des Hautes Energies, Ecole Polytechnique, IN²P³-CNRS, F-91128 Palaiseau Cedex, France

E. Focardi, G. Parrini, K. Zachariadou

Dipartimento di Fisica, Università di Firenze, INFN Sezione di Firenze, I-50125 Firenze, Italy

M. Corden, C. Georgiopoulos, D.E. Jaffe

Supercomputer Computations Research Institute, Florida State University, Tallahassee, FL 32306-4052, USA [13,14]

A. Antonelli, G. Bencivenni, G. Bologna,[4] F. Bossi, P. Campana, G. Capon, V. Chiarella, G. Felici, P. Laurelli, G. Mannocchi,[5] F. Murtas, G.P. Murtas, L. Passalacqua, M. Pepe-Altarelli

Laboratori Nazionali dell'INFN (LNF-INFN), I-00044 Frascati, Italy

L. Curtis, J.G. Lynch, P. Negus, V. O'Shea, C. Raine, J.M. Scarr, K. Smith, P. Teixeira-Dias, A.S. Thompson, E. Thomson

Department of Physics and Astronomy, University of Glasgow, Glasgow G12 8QQ,United Kingdom[10]

O. Buchmüller, S. Dhamotharan, C. Geweniger, G. Graefe, P. Hanke, G. Hansper, V. Hepp, E.E. Kluge, A. Putzer, J. Sommer, K. Tittel, S. Werner, M. Wunsch

  Institut für Hochenergiephysik, Universität Heidelberg, D-69120 Heidelberg, Germany[16]

R. Beuselinck, D.M. Binnie, W. Cameron, P.J. Dornan,[2] M. Girone, S. Goodsir, E.B. Martin, N. Marinelli, A. Moutoussi, J. Nash, J.K. Sedgbeer, P. Spagnolo, M.D. Williams

  Department of Physics, Imperial College, London SW7 2BZ, United Kingdom[10]

V.M. Ghete, P. Girtler, E. Kneringer, D. Kuhn, G. Rudolph

  Institut für Experimentalphysik, Universität Innsbruck, A-6020 Innsbruck, Austria[18]

A.P. Betteridge, C.K. Bowdery, P.G. Buck, P. Colrain, G. Crawford, A.J. Finch, F. Foster, G. Hughes, R.W.L. Jones, N.A. Robertson, M.I. Williams

  Department of Physics, University of Lancaster, Lancaster LA1 4YB, United Kingdom[10]

I. Giehl, C. Hoffmann, K. Jakobs, K. Kleinknecht, G. Quast, B. Renk, E. Rohne, H.-G. Sander, P. van Gemmeren, C. Zeitnitz

  Institut für Physik, Universität Mainz, D-55099 Mainz, Germany[16]

J.J. Aubert, C. Benchouk, A. Bonissent, G. Bujosa, J. Carr,[2] P. Coyle, F. Etienne, O. Leroy, F. Motsch, P. Payre, M. Talby, A. Sadouki, M. Thulasidas, K. Trabelsi

  Centre de Physique des Particules, Faculté des Sciences de Luminy, IN^2P^3-CNRS, F-13288 Marseille, France

M. Aleppo, M. Antonelli, F. Ragusa

  Dipartimento di Fisica, Università di Milano e INFN Sezione di Milano, I-20133 Milano, Italy

R. Berlich, V. Büscher, G. Cowan, H. Dietl, G. Ganis, G. Lütjens, C. Mannert, W. Männer, H.-G. Moser, S. Schael, R. Settles, H. Seywerd, H. Stenzel, W. Wiedenmann, G. Wolf

  Max-Planck-Institut für Physik, Werner-Heisenberg-Institut, D-80805 München, Germany[16]

J. Boucrot, O. Callot, S. Chen, A. Cordier, M. Davier, L. Duflot, J.-F. Grivaz, Ph. Heusse, A. Höcker, A. Jacholkowska, D.W. Kim,[12] F. Le Diberder, J. Lefrançois, A.-M. Lutz, M.-H. Schune, E. Tournefier, J.-J. Veillet, I. Videau, D. Zerwas

  Laboratoire de l'Accélérateur Linéaire, Université de Paris-Sud, IN^2P^3-CNRS, F-91898 Orsay Cedex, France

P. Azzurri, G. Bagliesi,[2] G. Batignani, S. Bettarini, T. Boccali, C. Bozzi, G. Calderini, M. Carpinelli, M.A. Ciocci, R. Dell'Orso, R. Fantechi, I. Ferrante, L. Foà,[1] F. Forti, A. Giassi, M.A. Giorgi, A. Gregorio, F. Ligabue, A. Lusiani, P.S. Marrocchesi, A. Messineo, F. Palla, G. Rizzo, G. Sanguinetti, A. Sciabà, G. Sguazzoni, R. Tenchini, G. Tonelli,[19] C. Vannini, A. Venturi, P.G. Verdini

  Dipartimento di Fisica dell'Università, INFN Sezione di Pisa, e Scuola Normale Superiore, I-56010 Pisa, Italy

G.A. Blair, L.M. Bryant, J.T. Chambers, M.G. Green, T. Medcalf, P. Perrodo, J.A. Strong, J.H. von Wimmersperg-Toeller

  Department of Physics, Royal Holloway & Bedford New College, University of London, Surrey TW20 OEX, United Kingdom[10]

D.R. Botterill, R.W. Clifft, T.R. Edgecock, P.R. Norton, J.C. Thompson, A.E. Wright

  Particle Physics Dept., Rutherford Appleton Laboratory, Chilton, Didcot, Oxon OX11 OQX, United Kingdom[10]

B. Bloch-Devaux, P. Colas, S. Emery, W. Kozanecki, E. Lançon,[2] M.-C. Lemaire, E. Locci, P. Perez, J. Rander, J.-F. Renardy, A. Roussarie, J.-P. Schuller, J. Schwindling, A. Trabelsi, B. Vallage

  CEA, DAPNIA/Service de Physique des Particules, CE-Saclay, F-91191 Gif-sur-Yvette Cedex, France[17]

S.N. Black, J.H. Dann, R.P. Johnson, H.Y. Kim, N. Konstantinidis, A.M. Litke, M.A. McNeil, G. Taylor

Institute for Particle Physics, University of California at Santa Cruz, Santa Cruz, CA 95064, USA[22]

C.N. Booth, S. Cartwright, F. Combley, M.S. Kelly, M. Lehto, L.F. Thompson

Department of Physics, University of Sheffield, Sheffield S3 7RH, United Kingdom[10]

K. Affholderbach, A. Böhrer, S. Brandt, C. Grupen, P. Saraiva, L. Smolik, F. Stephan

Fachbereich Physik, Universität Siegen, D-57068 Siegen, Germany[16]

G. Giannini, B. Gobbo, G. Musolino

Dipartimento di Fisica, Università di Trieste e INFN Sezione di Trieste, I-34127 Trieste, Italy

J. Rothberg, S. Wasserbaech

Experimental Elementary Particle Physics, University of Washington, WA 98195 Seattle, U.S.A.

S.R. Armstrong, E. Charles, P. Elmer, D.P.S. Ferguson, Y. Gao, S. González, T.C. Greening, O.J. Hayes, H. Hu, S. Jin, P.A. McNamara III, J.M. Nachtman,[23] J. Nielsen, W. Orejudos, Y.B. Pan, Y. Saadi, I.J. Scott, J. Walsh, Sau Lan Wu, X. Wu, G. Zobernig

Department of Physics, University of Wisconsin, Madison, WI 53706, USA[11]

1   Introduction

Flavour non-conservation in charged weak current interactions allows mixing between the B_s^0 and $\bar{B}_s^0$ flavour states. The proper-time probability density function of a B_s^0 meson which is known to have mixed oscillates. The oscillation frequency is proportional to Δm_s, the mass difference between the mass eigenstates. Within the framework of the Standard Model, a measurement of the ratio $\Delta m_s/\Delta m_d$ (Δm_d being the mass difference in the $B_d^0 - \bar{B}_d^0$ system) would allow the extraction of the ratio of Cabibbo-Kobayashi-Maskawa (CKM) quark mixing matrix elements $|V_{ts}/V_{td}|$.

Although the slower B_d^0 oscillations are now well established, the faster B_s^0 oscillations remain to be detected. Previous ALEPH analyses searching for B_s^0 oscillations have either been based on semi-exclusive selections in which a D_s^- is fully reconstructed [1, 2] or on more inclusive lepton selections [3, 4, 5]. Although the latter suffer from a lower B_s^0 purity and poorer proper time resolution they have the advantage of larger statistics.

The analysis presented here is also based on an inclusive lepton sample. Compared to the previous ALEPH inclusive lepton analysis [4], the following improvements are made to increase the sensitivity to B_s^0 mixing.

- **Decay length resolution:** An improved decay length resolution is obtained by applying tight selection cuts to remove events likely to have misassigned tracks between the primary and the B_s^0 vertex. In addition an estimate of the decay length uncertainty is used on an event-by-event basis, rather than assuming the same average decay length uncertainty for all events, as used in previous analyses.

- **Boost resolution:** A nucleated jet algorithm is used for an improved estimate of the momentum of the b-hadrons.

- **B_s^0 purity classes:** Various properties of the events, such as the charge of the reconstructed b-hadron vertex and the presence of kaons are used to enhance the fraction of B_s^0 in subsamples of the data.

- **Initial and final state tagging:** The b-flavour tagging method previously used for the D_s^- based analyses [1, 2] is applied. In this method discriminating variables are used to construct mistag probabilities and sample composition fractions estimated on an event-by-event basis. As a result, all events are tagged and the effective mistag rate is reduced.

This paper details these improvements and is organized as follows. After a brief description of the ALEPH detector, the event selection is described in Section 3 and the B_s^0 purity classification procedure in Section 4. The next two sections explain the proper time reconstruction and the procedure for tagging the initial and final state b quark charge. The likelihood function is presented in Section 7 and the Δm_s results in Section 8. In Section 9 the systematic uncertainties are described, and in Section 10 additional checks of the analysis presented. Finally the combination of this analysis with the ALEPH D_s^- based analyses is described in Section 11.

2 The ALEPH detector

The ALEPH detector and its performance from 1991 to 1995 are described in detail elsewhere [6, 7], and only a brief overview of the apparatus is given here. Surrounding the beam pipe, a high resolution vertex detector (VDET) consists of two layers of double-sided silicon microstrip detectors, positioned at average radii of 6.5 cm and 11.3 cm, and covering 85% and 69% of the solid angle respectively. The spatial resolution for the $r\phi$ and z projections (transverse to and along the beam axis, respectively) is 12 μm at normal incidence. The vertex detector is surrounded by a drift chamber with eight coaxial wire layers with an outer radius of 26 cm and by a time projection chamber (TPC) that measures up to 21 three-dimensional points per track at radii between 30 cm and 180 cm. These detectors are immersed in an axial magnetic field of 1.5 T and together measure the momenta of charged particles with a resolution $\sigma(p)/p = 6 \times 10^{-4} p_{\mathrm{T}} \oplus 0.005$ (p_{T} in GeV$/c$). The resolution of the three-dimensional impact parameter in the transverse and longitudinal view, for tracks having information from all tracking detectors and two VDET hits (a VDET "hit" being defined as having information from both $r\phi$ and z views), can be parametrized as $\sigma = 25\,\mu\mathrm{m} + 95\,\mu\mathrm{m}/p$ (p in GeV$/c$). The TPC also provides up to 338 measurements of the specific ionization of a charged particle. In the following, the dE/dx information is considered as available if more than 50 samples are present. Particle identification is based on the dE/dx estimator χ_π (χ_{K}), defined as the difference between the measured and expected ionization expressed in terms of standard deviations for the π (K) mass hypothesis. The TPC is surrounded by a lead/proportional-chamber electromagnetic calorimeter segmented into $0.9° \times 0.9°$ projective towers and read out in three sections in depth, with energy resolution $\sigma(E)/E = 0.18/\sqrt{E} + 0.009$ (E in GeV). The iron return yoke of the magnet is instrumented with streamer tubes to form a hadron calorimeter, with a thickness of over 7 interaction lengths and is surrounded by two additional double-layers of streamer tubes to aid muon identification. An algorithm combines all these measurements to provide a determination of the energy flow [7] with an uncertainty on the total measurable energy of $\sigma(E) = (0.6\sqrt{E/\mathrm{GeV}} + 0.6)$ GeV.

3 Event selection

This analysis uses approximately 4 million hadronic Z events recorded by the ALEPH detector from 1991 to 1995 at centre of mass energies close to the Z peak and selected with the charged particle requirements described in Ref. [8]. It relies on Monte Carlo samples of fully simulated Z $\rightarrow$ q$\bar{\mathrm{q}}$ events. The Monte Carlo generator is based on JETSET 7.4 [9] with updated branching ratios for heavy flavour decays. Monte Carlo events are reweighted to the physics parameters listed in Table 1.

Events for which the cosine of the angle between the thrust axis and the beam axis is less than 0.85 are selected. Using the plane perpendicular to the thrust axis, the event is split into two hemispheres. Electrons and muons are identified using the standard ALEPH lepton selection criteria [10]. Events containing at least one such lepton with momentum above 3 GeV$/c$ are kept. The leptons are then associated to their closest jet (constructed using the JADE algorithm [11] with $y_{\mathrm{cut}} = 0.004$) and a transverse momentum p_T with respect to the jet is calculated with the lepton momentum removed from the jet. Only

leptons with $p_T > 1.25$ GeV/c are selected. In the case that more than one lepton in an event satisfies this requirement, only the lepton with the highest momentum is used as a candidate for a B_s^0 decay product.

The e^+e^- interaction point is reconstructed on an event-by-event basis using the constraint of the average beam spot position and envelope [12].

A charm vertex is then reconstructed in the lepton hemisphere using the algorithm described in Ref. [3]. Charged particles in this hemisphere (other than the selected lepton) are assigned to either the interaction point or a single displaced secondary vertex. A three-dimensional grid search is performed for the secondary vertex position to find the combination of assignments that has the greatest reduction in χ^2 as compared to the case when all tracks are assumed to come from the interaction point. Tracks are required to come within 3σ of their assigned vertex. The position resolution of this "charm vertex" is subsequently improved by removing those tracks having a momentum below 1.5 GeV/c or an impact parameter significance relative to the charm vertex larger than 1.4σ. The remaining tracks are then re-vertexed to form the reconstructed "charm particle". If only one track passes the requirements, it serves as the charm particle. The event is rejected if no track remains, or none of the tracks assigned to the charm vertex have at least one vertex detector hit. The charm particle is then combined with the lepton to form a candidate b-hadron vertex. The lepton is required to have at least one vertex detector hit and the χ^2 per degree of freedom of the reconstructed b-hadron vertex is required to be less than 25.

The energy E_c of the charm particle is estimated by clustering a jet, using the JADE algorithm, around the charged tracks at the charm vertex until a mass of 2.7 GeV/c^2 is reached. To reduce the influence of fragmentation particles on the estimate of E_c, charged and neutral particles with energies less than 0.5 GeV are excluded from the clustering [16]. The neutrino energy E_ν is estimated from the missing energy in the lepton hemisphere taking into account the measured mass in each hemisphere [17]. Assuming the direction of flight of the b-hadron to be that of its associated jet, an estimate of the b-hadron mass can be calculated from the energy of the neutrino and the four-vectors of the charm particle and the lepton.

In order to improve the rejection of non-b background or b events with a badly estimated decay length error, the following additional cuts are applied [18]:

- the momentum of the charm particle must be larger than 4 GeV/c; this cut is increased to 8 GeV/c when the angle between the charm particle and the lepton is less than 10°;

- the reconstructed mass of the b-hadron must be less than 8 GeV/c^2;

- the missing energy in the lepton hemisphere must be larger than -2 GeV;

- the angle between the charm particle and the lepton must be between 5° and 30°;

- the angle between the charm particle and the jet must be less than 20°.

Although the total efficiency of these additional requirements is 35%, the average decay length resolution of the remaining events is improved by a factor of 2 and the amount of non-b background in the sample reduced by a factor close to 4. In addition the average

Table 1: Values of the physics parameters assumed in this analysis.

Physics parameter	Value and uncertainty	Reference
B_s^0 lifetime	1.49 ± 0.06 ps	[13]
B_d^0 lifetime	1.57 ± 0.04 ps	[13]
B^+ lifetime	1.67 ± 0.04 ps	[13]
b-baryon lifetime	1.22 ± 0.05 ps	[13]
Δm_d	0.463 ± 0.018 ps^{-1}	[13]
$R_b = \mathcal{B}(Z \to b\bar{b})/\mathcal{B}(Z \to q\bar{q})$	0.2170 ± 0.0009	[14]
$R_c = \mathcal{B}(Z \to c\bar{c})/\mathcal{B}(Z \to q\bar{q})$	0.1733 ± 0.0048	[14]
$f_{B_s^0} = \mathcal{B}(\bar{b} \to B_s^0)$	$0.103^{+0.016}_{-0.015}$	[13]
$f_{B_d^0} = f_{B^+} = \mathcal{B}(\bar{b} \to B_d^0, B^+)$	$0.395^{+0.016}_{-0.020}$	[13]
$f_{\text{b-baryon}} = \mathcal{B}(b \to \text{b-baryon})$	$0.106^{+0.037}_{-0.027}$	[13]
$\mathcal{B}(b \to \ell)$	0.1112 ± 0.0020	[14]
$\mathcal{B}(b \to c \to \ell)$	0.0803 ± 0.0033	[14]
$\mathcal{B}(b \to \bar{c} \to \ell)$	0.0013 ± 0.0005	[15]
$\mathcal{B}(c \to \ell)$	0.098 ± 0.005	[15]
$\langle X_E \rangle$	0.702 ± 0.008	[15]

Table 2: Lepton candidate sources (%), as estimated from Monte Carlo. Quoted uncertainties are statistical only.

B_s^0	B_d^0	other b-hadrons	charm	uds
10.35 ± 0.08	38.53 ± 0.13	47.86 ± 0.14	2.31 ± 0.06	0.95 ± 0.05

momentum resolution of the sample is significantly improved. A total of 33023 events survive after all cuts.

4 B_s^0 purity classes

Table 2 shows the composition of the final event sample obtained assuming the physics parameters listed in Table 1 and reconstruction efficiencies determined from Monte Carlo. The average B_s^0 purity in the sample is estimated to be 10.35%.

The sensitivity of the analysis to B_s^0 mixing is increased by splitting the data into subsamples with a B_s^0 purity larger or smaller than the average and then making use of this knowledge in the likelihood fit. Classes are constructed based on (i) the track multiplicity at the charm vertex, (ii) the number of identified kaon candidates and (iii) the charge correlation between the tracks at the charm vertex and the lepton. The definition of the eleven classes used in this analysis is given in Table 3. As the last class contains those events which do not satisfy the criteria of the preceding classes, the classification procedure does not reject events.

For an odd (even) number of charged tracks assigned to the charm vertex, the

Table 3: Definition of the eleven B_s^0 purity classes. Column 1 gives the number of charged tracks at the charm vertex. Column 2 shows whether the charge of these tracks are the same (S) or opposite (O) to that of the lepton, the tracks being ranked in order of decreasing momentum. Column 3 indicates the subclasses based on the presence of kaon or ϕ candidates at the charm vertex. Column 4 shows the fraction of data events in each class. Column 5 gives the B_s^0 purity in each class, as estimated from Monte Carlo. Quoted uncertainties are statistical only.

Number of tracks	Charge correlation	Kaon requirements	Fraction in data (%)	B_s^0 purity (%)
1	O	1 kaon	3.8	24.0 ± 0.6
		0 kaon	14.9	14.7 ± 0.3
2	OS, SO	ϕ	1.2	21.1 ± 1.0
	OS, SO	0 kaon	17.8	7.0 ± 0.2
	OS, SO	1 kaon	17.4	5.2 ± 0.1
	OS, SO	2 kaons	2.3	8.4 ± 0.5
	OO		8.3	16.7 ± 0.4
3	OOS		2.9	19.4 ± 0.6
	OSO		3.8	18.0 ± 0.5
	SOO		3.9	14.5 ± 0.5
remainder			23.6	5.7 ± 0.1

reconstructed charge of the b-hadron vertex is more likely to be zero (non-zero), and therefore the probability for the hemisphere to contain a neutral b-hadron is enhanced (reduced). For events having two oppositely charged tracks at the charm vertex, the B_s^0 purity is 6.7%, which is lower than the average purity. For this large subsample of events, the presence of kaon candidates and consistency with the ϕ mass are used to recover some sensitivity to the B_s^0. In this procedure, kaon candidates are defined as charged tracks with momentum above 2 GeV/c satisfying $\chi_\pi + \chi_K < 0$ and $|\chi_K| < 2$, and a ϕ candidate is defined as a pair of oppositely charged tracks with an invariant mass between 1.01 and 1.03 GeV/c^2 (assuming kaon masses for the two tracks).

Monte Carlo studies indicate that this classification procedure is effectively equivalent to increasing the statistics of the sample by 28%.

5 Proper time reconstruction and resolution

An estimate, l, of the decay length of each b-hadron candidate is calculated as the distance from the interaction point to the b-hadron vertex projected onto the direction of the jet associated to the lepton. This decay length includes a global correction of -78 μm, determined using Monte Carlo events. This small offset is due to the vertex reconstruction algorithm, which assumes that all lepton candidates in b events come from direct b $\to \ell$ decays. Figure 1a shows the Monte Carlo distribution of $l - l_0$ for b events, where l_0 is the true decay length. An event-by-event decay length uncertainty, σ_l, is estimated from the covariance matrices of the tracks attached to the vertices. This can be compared with the true error, $(l - l_0)$, by constructing the pull distribution, $(l - l_0)/\sigma_l$. A fit to this Monte
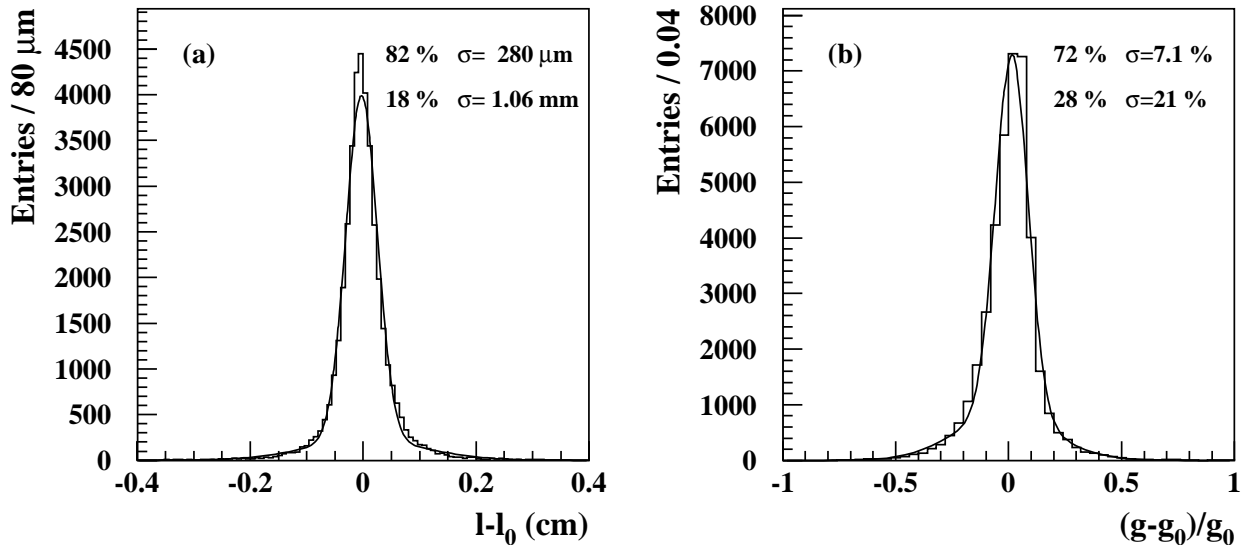
Figure 1: Decay length resolution (a) and relative boost term resolution (b) for all b-hadrons; the curves are the result of fits of the sum of two Gaussian functions with relative fractions and widths as indicated.

Table 4: Double-Gaussian parametrizations of the decay length pull and relative boost term resolution obtained from Monte Carlo.

Parametrization of $(l - l_0)/\sigma_l$				Parametrization of $(g - g_0)/g_0$		
α	Fraction f_l^α	Sigma S_l^α		β	Fraction f_g^β	Sigma S_g^β
1	0.849 ± 0.003	1.333 ± 0.005		1	0.723 ± 0.004	0.0713 ± 0.0003
2	0.151 ± 0.003	4.365 ± 0.033		2	0.277 ± 0.004	0.2101 ± 0.0012

Carlo distribution of the sum of two Gaussian functions ($\alpha = 1, 2$) yields the fractions, f_l^α, and sigmas, S_l^α, indicated in Table 4. These parameters are used to describe the observed tails when constructing the resolution function.

The true boost term is defined as $g_0 = t_0/l_0$, where t_0 is the true proper time. An estimate of the boost term is formed using $g = m_B/p_B + 0.36$ ps/cm. The average b-hadron mass, m_B, is assumed to be 5.3 GeV/c^2 and the reconstructed momentum is calculated as $p_B = \sqrt{(E_c + E_\nu + E_\ell)^2 - m_B^2}$ where E_ℓ is the measured lepton energy. The constant term is an average offset correction determined using Monte Carlo events; this results from the choice of the mass cut-off used in the nucleated jet algorithm described in Section 3, which optimizes the relative boost term resolution. The distribution of $(g - g_0)/g_0$, shown in Fig. 1b, is parametrized with the sum of two Gaussian functions; Table 4 shows the corresponding fractions, f_g^β, and sigmas, S_g^β, determined with Monte Carlo events.

The proper time of each b-hadron candidate is computed from the estimated decay length and boost term as

$$t = l\,g\,,\tag{1}$$

and its proper time resolution function is parametrized with the sum of four Gaussian
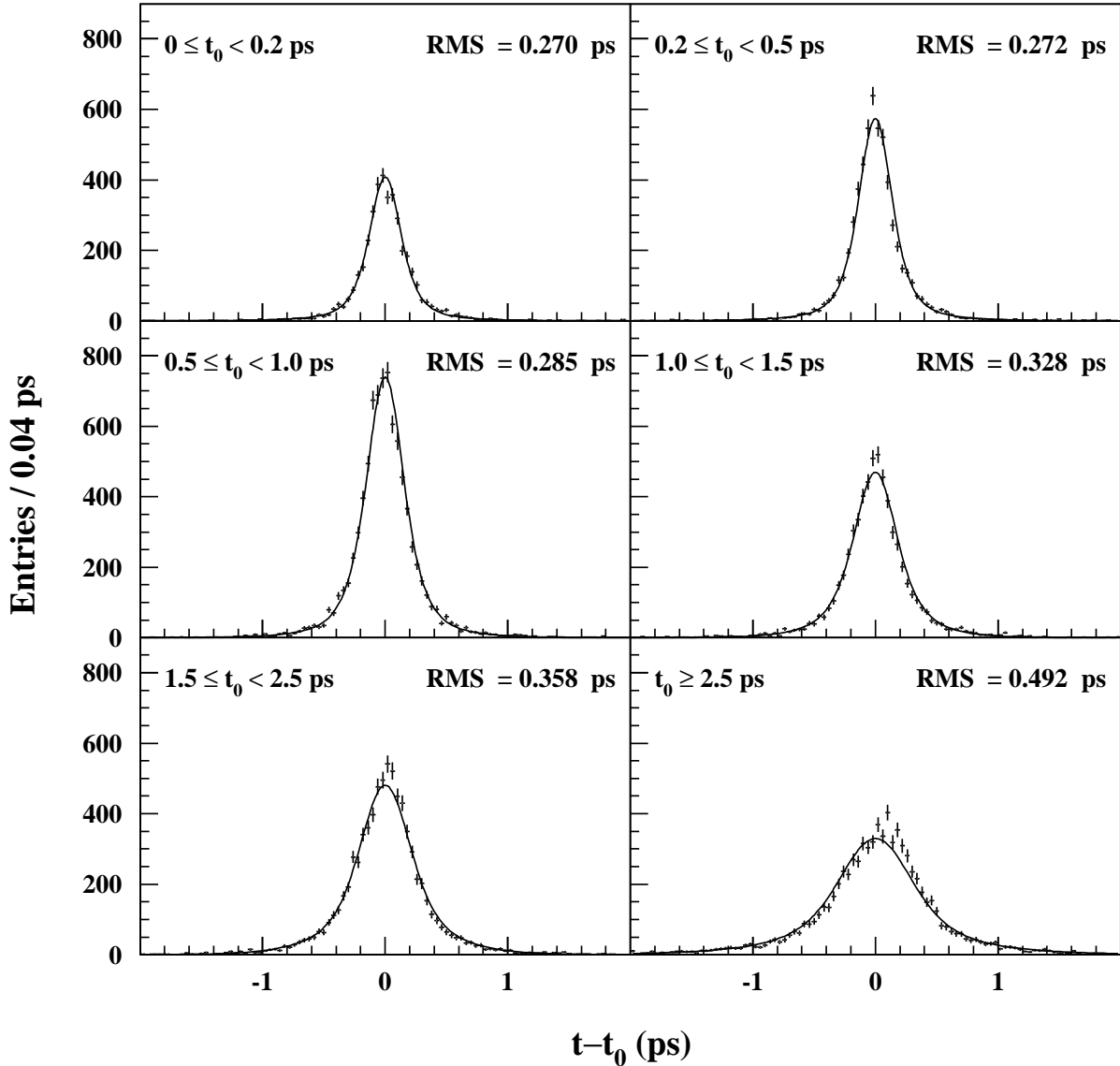
Figure 2: The proper time resolution for b events in various intervals of true proper time t_0 (in ps). The curves display the corresponding resolution assumed in the likelihood as obtained from Eq. (2). The RMS values indicated, are derived from the data points shown.

components,

$$\mathrm{Res}(t, t_0) = \sum_{\alpha=1}^{2} \sum_{\beta=1}^{2} f_l^{\alpha'} f_g^{\beta} \frac{1}{\sqrt{2\pi}\sigma^{\alpha\beta}(t_0)} \exp\left[-\frac{1}{2}\left(\frac{t - t_0}{\sigma^{\alpha\beta}(t_0)}\right)^2\right], \qquad (2)$$

where $f_l^{2'} = f_l^{\mathrm{dat}} f_l^2$ and $f_l^{1'} = 1 - f_l^{2'}$, and where the event-by-event resolution $\sigma^{\alpha\beta}$ of each component, given by

$$\sigma^{\alpha\beta}(t_0) = \sqrt{\left(g S_l^{\mathrm{dat}} S_l^{\alpha} \sigma_l\right)^2 + \left(t_0 S_g^{\mathrm{dat}} S_g^{\beta}\right)^2}, \qquad (3)$$

includes the explicit dependence on t_0. This parametrization implicitly assumes that any

7

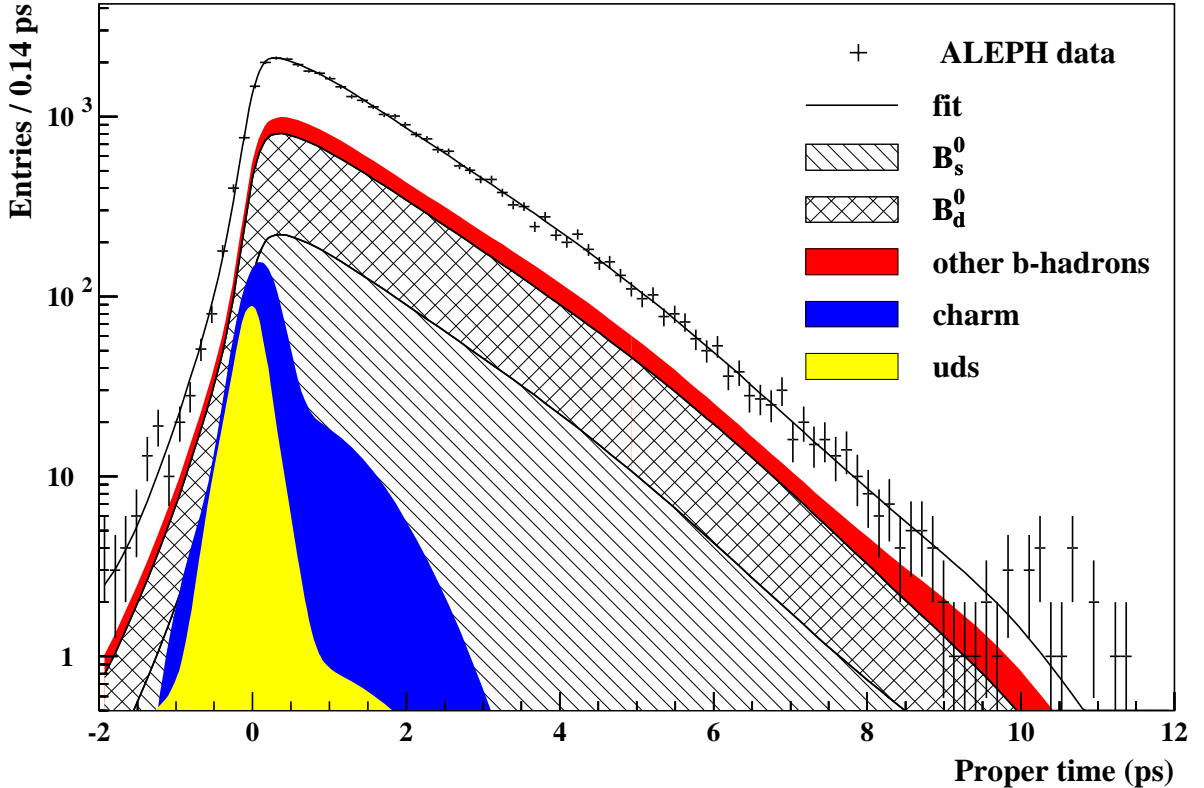Figure 3: The reconstructed proper time distributions of the selected events in data. The contributions from the various components are indicated. The curve is the result of the fit described in Section 5.

correlation between the decay length resolution and the relative boost resolution is small, as confirmed by Monte Carlo studies.

The scale factors S_l^{dat} and f_l^{dat} are introduced to account for a possible discrepancy between data and Monte Carlo, both in the amount of tail in the decay length pull (f_l^{dat}) and in the estimate of σ_l itself (S_l^{dat}). In a similar fashion, the inclusion of the parameter S_g^{dat} allows possible systematic uncertainties due to the boost resolution to be studied. By definition all these factors are set to unity when describing the resolution of simulated events. Figure 2 shows, for various intervals of true proper time, the proper time resolution of simulated b events together with the parametrization obtained from Eq. (2). The parametrization is satisfactory, especially for small proper times.

In order to measure S_l^{dat} and f_l^{dat} in the data, a fit is performed to the reconstructed proper time distribution of the selected sample of real events. This is performed using the likelihood function described in Section 7, modified to ignore tagging information. Fixing all physics parameters to their central values given in Table 1, the likelihood is maximized with respect to S_l^{dat} and f_l^{dat}. The fit reproduces well the negative tail of the proper time distribution (see Fig. 3), showing that the resolution is satisfactorily described by the chosen parametrization. The fitted values $S_l^{\mathrm{dat}} = 1.02 \pm 0.03$ and $f_l^{\mathrm{dat}} = 1.20 \pm 0.09$ indicate that the decay length resolution in the data is somewhat worse than that suggested by the Monte Carlo simulation.
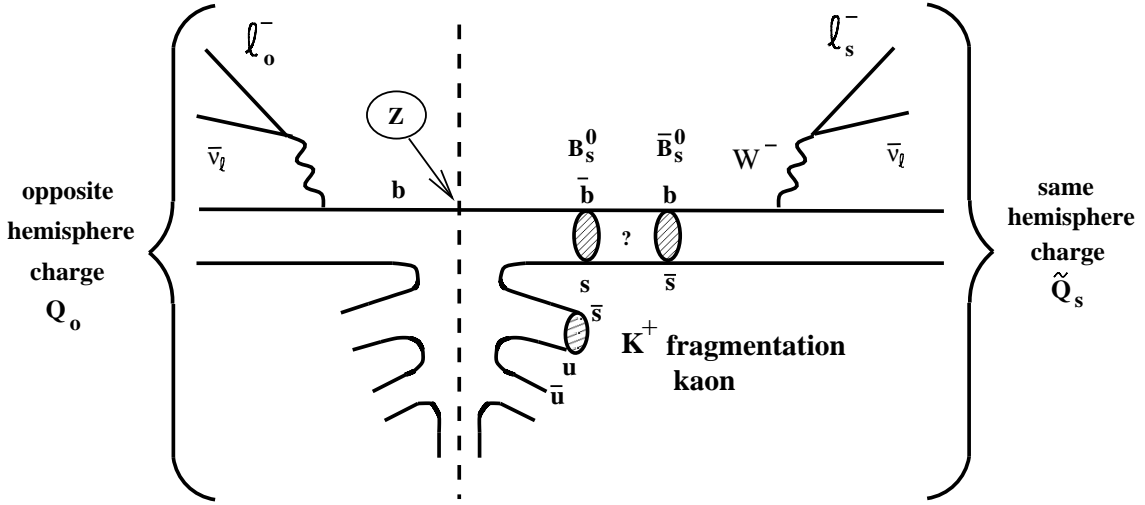
Figure 4: Schematic drawing indicating the initial and final state tags used in this analysis.

6 Initial and final state tagging

The flavour state of the decaying B_s^0 candidate is estimated from the charge of the reconstructed lepton. This final state tag is incorrect if the lepton is from the $b \to c \to \ell$ decay (6.1% of the b events in the sample) as the charge of the lepton is reversed. The flavour state at production is estimated using three initial state tags. A B_s^0 candidate is "tagged as unmixed (mixed)" when the reconstructed initial and final flavour states are the same (different). By definition, candidates from charm, uds, or non-oscillating b-hadron backgrounds are correctly tagged if they are tagged as unmixed.

The tagging power is enhanced by the means of discriminating variables which have some ability to distinguish between correctly tagged and incorrectly tagged candidates. This approach was first used in the ALEPH D_s^-–lepton analysis [1] and refined for the D_s^-–hadron analysis [2]. In contrast to what was performed in Refs. [1] and [2], an event is considered to be mistagged if either the initial or final state is incorrectly tagged, but not both.

For each B_s^0 candidate, one of the tags described below is used to determine the initial state (see also Fig. 4).

- **Opposite lepton tag:** Leptons with momentum larger than 3 GeV/c are searched for in the hemisphere opposite to the B_s^0 candidate. The sign of the lepton with the highest transverse momentum $p_T(\ell_o)$ tags the nature of the initial b quark in the opposite hemisphere. It takes precedence over the other tags if it is available.

- **Fragmentation kaon tag:** The fragmentation kaon candidate is defined as the highest momentum charged track within 45° of the B_s^0 direction, identified, using the vertexing algorithm described in Section 2, as being more likely to come from the interaction point than the charm vertex, and satisfying $\chi_K < 0.5$ and $\chi_K - \chi_\pi > 0.5$.

The sign of the fragmentation kaon candidate tags the sign of the b quark in the same hemisphere. It is used if no opposite hemisphere lepton tag is found.

- **Opposite hemisphere charge tag:** The opposite hemisphere charge is defined as

$$Q_{\mathrm{o}} = \frac{\sum\limits_{i}^{\mathrm{oppo}} q_i \, |p_{\parallel}^i|^{\kappa}}{\sum\limits_{i}^{\mathrm{oppo}} |p_{\parallel}^i|^{\kappa}} \,, \tag{4}$$

where the sum is over all charged particles in the opposite hemisphere, $p_{\parallel}^i$ is the momentum of the ith track projected on the thrust axis, q_i its charge and $\kappa = 0.5$. The sign of Q_{o} tags the initial state of the b quark in the opposite hemisphere. This tag is always available but has the largest mistag probability of the three tags. It is used only if no other tag is available.

The events are sorted into five exclusive classes based on the availability and results of the three tags. The definition of these tagging classes and the list of the discriminating variables associated with each class are given in Table 5. The variable $\tilde{Q}_{\mathrm{s}}$ is the sum of the charges of all the tracks in the same hemisphere and carries information on the initial state of the B_{s}^0. As the sum of charges of tracks originating from the decay of a neutral particle is zero, it is independent of whether the B_{s}^0 decays as a B_{s}^0 or a $\bar{B}_{\mathrm{s}}^0$. The variable Z_{K} is defined as $Z_{\mathrm{K}} = p_{\mathrm{K}}/(E_{\mathrm{beam}} - E_{\mathrm{B}})$, where p_{K} is the kaon momentum, E_{beam} the beam energy and E_{B} the B_{s}^0 candidate energy. The inclusion of the reconstructed B_{s}^0 proper time t takes into account that the mistag probability of the fragmentation kaon tag increases as the B_{s}^0 vertex approaches the primary vertex, due to the misassignment of tracks between the primary and secondary vertices. The use, for all classes, of the variable $p_T(\ell_{\mathrm{s}})$, the transverse momentum of the lepton from the B_{s}^0 candidate decay, reduces the deleterious effect of $b \to c \to \ell$ on the final state mistag.

The mistag probability, η, for the B_{s}^0 signal events in each class, as well as the probability distributions of each discriminating variable x_i for correctly and incorrectly tagged signal events, $r_i(x_i)$ and $w_i(x_i)$, are estimated from Monte Carlo. The various discriminating variables chosen in each class, $x_1, x_2, \ldots$, are combined into a single effective discriminating variable x^{eff}, according to the prescription developed for the D_{s}^- based analyses [1, 2]. This new variable is defined as

$$x^{\mathrm{eff}} = \frac{\eta \, w_1(x_1) \, w_2(x_2) \, \cdots}{(1 - \eta) \, r_1(x_1) \, r_2(x_2) \, \cdots + \eta \, w_1(x_1) \, w_2(x_2) \, \cdots} \,, \tag{5}$$

and takes values between 0 and 1. A small value indicates that the B_{s}^0 oscillation is likely to have been correctly tagged.

To allow use of the discriminating variables in the likelihood fit, the probability density functions $G_{jkl}^c(x^{\mathrm{eff}})$ of x^{eff} are determined for each lepton source j, in each tagging class k and in each B_{s}^0 purity class l, separately for the correctly ($c = +1$) and incorrectly ($c = -1$) tagged events. This determination (as well as the estimation of the corresponding mistag probabilities η_{jkl}) is based on Monte Carlo.

The enhancement of the tagging power provided by the variable, x^{eff}, depends on the difference between the $G_{jkl}^+(x^{\mathrm{eff}})$ and $G_{jkl}^-(x^{\mathrm{eff}})$ distributions, and can be quantified in

Table 5: The tag and discriminating variables used in each class. The quantities $S(Q_o)$, $S(K)$ and $S(\ell_o)$ are the signs of the opposite hemisphere charge, the fragmentation kaon and the opposite side lepton. Classes 3–5 all use the sign of the opposite hemisphere lepton as the initial state tag. For Class 3 no fragmentation kaon candidate is identified. For Class 4 (Class 5) a fragmentation kaon candidate is found whose charge is the same as (opposite to) the charge of the opposite hemisphere lepton. Purity and mistag rates are estimated from Monte Carlo. Quoted uncertainties are statistical only.

Tagging class	1	2	3	4	5
Available initial state tags	$S(Q_o)$	$S(Q_o)$ $S(K)$	$S(Q_o)$ $S(\ell_o)$	$S(Q_o)$ $S(\ell_o)=-S(K)$	$S(Q_o)$ $S(\ell_o)=S(K)$
Intial state tag used	$S(Q_o)$	$S(K)$	$S(\ell_o)$	$S(\ell_o)=-S(K)$	$S(\ell_o)=S(K)$
Discriminating variables used	$\|Q_o\|$ $S(Q_o)\tilde{Q}_s$ $p_T(\ell_s)$	$S(K)Q_o$ $S(K)\tilde{Q}_s$ χ_π Z_K t $p_T(\ell_s)$	$S(\ell_o)Q_o$ $S(\ell_o)\tilde{Q}_s$ $p_T(\ell_o)$ $p_T(\ell_s)$	χ_π Z_K $S(\ell_o)Q_o$ $S(\ell_o)\tilde{Q}_s$ $p_T(\ell_o)$ t $p_T(\ell_s)$	χ_π Z_K $S(\ell_o)Q_o$ $S(\ell_o)\tilde{Q}_s$ $p_T(\ell_o)$ t $p_T(\ell_s)$
Fraction in data (%)	71.4 ± 0.2	11.9 ± 0.2	14.2 ± 0.2	1.3 ± 0.1	1.2 ± 0.1
B_s^0 purity (%)	9.8 ± 0.1	13.1 ± 0.3	10.1 ± 0.2	15.6 ± 1.0	11.8 ± 0.8
B_s^0 mistag (%)	38.6 ± 0.5	28.9 ± 1.0	34.0 ± 1.1	16.1 ± 2.3	55.9 ± 3.5
B_s^0 effective mistag (%)	32.4	24.0	24.5	12.5	22.3
B_d^0 mistag (%)	38.4 ± 0.2	48.5 ± 0.7	35.4 ± 0.5	35.5 ± 2.0	39.9 ± 2.0
other B mistag (%)	37.6 ± 0.2	61.4 ± 0.5	34.2 ± 0.5	43.8 ± 1.8	24.1 ± 1.4
charm mistag (%)	38.2 ± 1.4	54.2 ± 3.2	14.2 ± 3.1	50.0 ± 50.0	8.6 ± 8.2
uds mistag (%)	47.8 ± 2.8	56.9 ± 6.0	46.0 ± 12.9	50.0 ± 50.0	50.0 ± 50.0

terms of effective mistag rates, as described in Ref. [1]. The effective mistag rates for the B_s^0 signal in the five tagging classes are given in Table 5. This table also indicates B_s^0 purity and the mistags for all background components. The overall average B_s^0 effective mistag is 29%.

Figure 5 displays the distribution of x^{eff} in each of the tagging classes; a good agreement is observed between data and Monte Carlo. The systematic uncertainties associated with the tagging procedure are considered in Section 9.
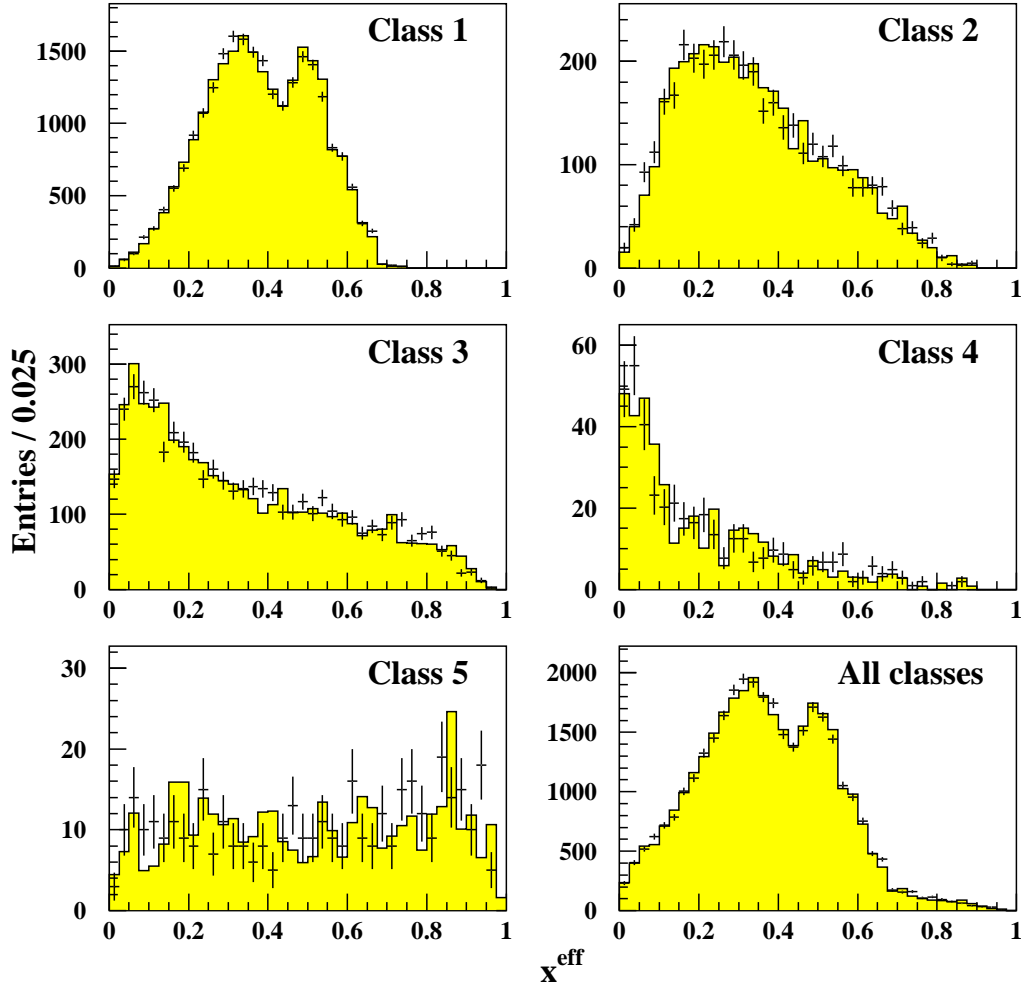
11

Figure 5: Distribution of x^{eff} in each tagging class in data (points) and Monte Carlo (histogram).

7 Likelihood function

Each b-hadron source has a different probability distribution function for the true proper time, t_0, and for the discrete variable, μ_0, defined to take the value -1 for the mixed case or $+1$ for the unmixed case. Assuming CP conservation and equal decay widths for the two CP eigenstates in each neutral B-meson system, the joint probability distribution of t_0 and μ_0 can be written as

$$p_j(\mu_0, t_0) = \frac{e^{-t_0/\tau_j}}{2\tau_j} \left[1 + \mu_0 \cos\left(\Delta m_j\, t_0\right)\right] , \qquad (6)$$

where τ_j and Δm_j are the lifetime and oscillation frequency of b-hadron source j (with the convention that $\Delta m_j = 0$ for non-oscillating b-hadrons).

The efficiency for reconstructing the b-hadron vertex depends on the true proper time. The stringent selection cuts described in Section 3 are designed to reduce the fraction of

12

fragmentation tracks assigned to the charm vertex, consequently causing a loss of efficiency at small proper times. Similarly at large proper times the efficiency also decreases as one is less likely to include a fragmentation track at the charm vertex and therefore more likely to fail the requirement of the charm vertex being assigned at least one track. The efficiencies $\epsilon_j(t_0)$ are parametrized separately for each b-hadron component j. They are independent of whether the b-hadron candidate is tagged as mixed or unmixed.

The joint probability distribution of the reconstructed proper time t and of μ_0 is obtained as the convolution of $p_j(\mu_0, t_0)$ with the event-by-event resolution function $\mathrm{Res}(t, t_0)$ (Section 5) and takes into account the observed dependence of the selection efficiency on true proper time:

$$h_j(\mu_0, t) = \frac{\int_0^\infty \epsilon_j(t_0) p_j(\mu_0, t_0) \mathrm{Res}(t, t_0)\, dt_0}{\int_0^\infty \epsilon_j(t_0) \frac{1}{\tau_j} e^{-t_0/\tau_j}\, dt_0}\,. \tag{7}$$

For the lighter quark backgrounds, $h_j(-1, t) = 0$ as these sources are unmixed by definition, and $h_j(+1, t)$ are the reconstructed proper time distributions. These distributions are determined from Monte Carlo samples and are parametrized as the sum of three Gaussian functions.

The likelihood function used in this analysis is based on the values taken by three different variables in the selected data events. These variables are the reconstructed proper time t, the tagging result μ, taking the value -1 for events tagged as mixed or $+1$ for those tagged as unmixed, and the effective discriminating variable x^{eff}. The use of the discriminating variable x^{eff} in the likelihood function is reduced to the use of two sets of functions of x^{eff}, $X_{jkl}(x^{\mathrm{eff}})$ and $Y_{jkl}(x^{\mathrm{eff}})$ (described below), whose values can be interpreted as event-by-event mistag probabilities and fractions of the different lepton sources respectively. The likelihood of the total sample is written as

$$\mathcal{L} = C \prod_l^{11\ \mathrm{purity}} \prod_k^{5\ \mathrm{tagging}} \prod_i^{N_{kl}\ \mathrm{events}} f_{kl}\left(x^{\mathrm{eff}}_{ikl}, \mu_{ikl}, t_{ikl}\right), \tag{8}$$

where C is a constant independent of b-hadron oscillation frequencies and lifetimes, N_{kl} is the number of selected candidates from $\mathrm{B}_{\mathrm{s}}^0$ purity class l falling in tagging class k, and where

$$f_{kl}(x^{\mathrm{eff}}, \mu, t) = \sum_j^{5\ \mathrm{sources}} Y_{jkl}(x^{\mathrm{eff}}) \left[\left(1 - X_{jkl}(x^{\mathrm{eff}})\right) h_j(\mu, t) + X_{jkl}(x^{\mathrm{eff}}) h_j(-\mu, t)\right] \tag{9}$$

sums over the 5 different lepton sources considered to comprise the sample (see Table 2). The event-by-event quantities $X_{jkl}(x^{\mathrm{eff}})$ and $Y_{jkl}(x^{\mathrm{eff}})$ are computed from the distributions $G_{jkl}^c(x^{\mathrm{eff}})$ and mistag probabilities η_{jkl} introduced in Section 6,

$$X_{jkl}(x^{\mathrm{eff}}) = \eta_{jkl}\, \frac{G_{jkl}^-(x^{\mathrm{eff}})}{G_{jkl}(x^{\mathrm{eff}})}\,, \quad Y_{jkl}(x^{\mathrm{eff}}) = \alpha_{jkl}\, \frac{G_{jkl}(x^{\mathrm{eff}})}{\sum_{j'} \alpha_{j'kl} G_{j'kl}(x^{\mathrm{eff}})}\,, \tag{10}$$

where $G_{jkl}(x^{\mathrm{eff}}) = (1 - \eta_{jkl}) G_{jkl}^+(x^{\mathrm{eff}}) + \eta_{jkl} G_{jkl}^-(x^{\mathrm{eff}})$ and where α_{jkl} are the source fractions, satisfying $\sum_{j=1}^{5\ \mathrm{sources}} \alpha_{jkl} = 1$.
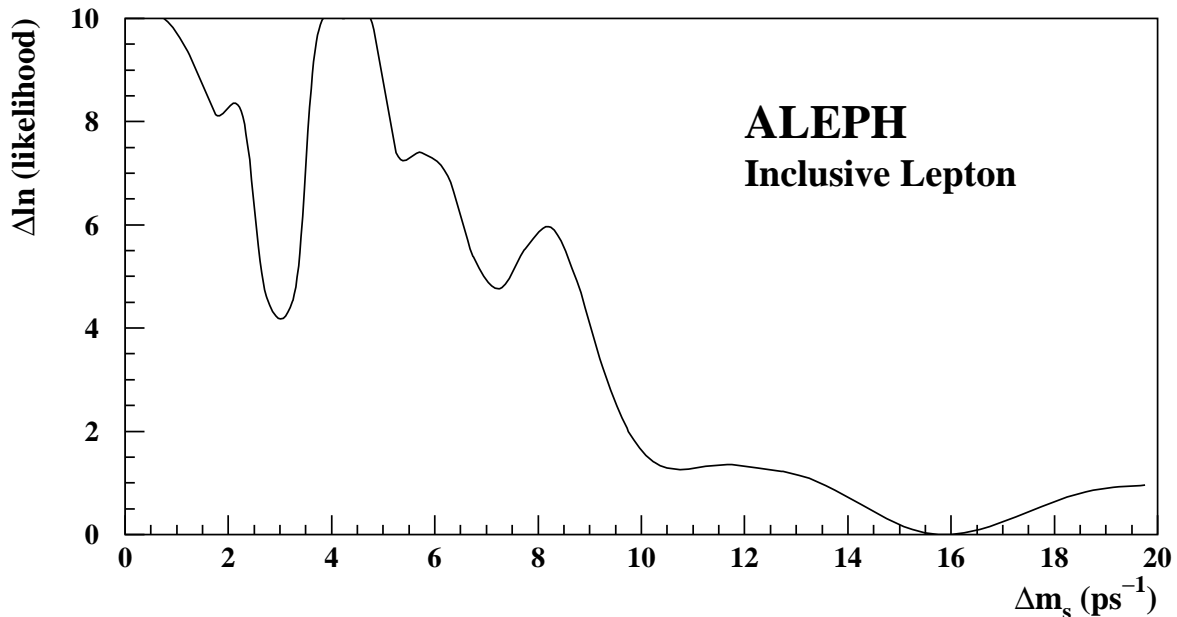
13

Figure 6: Negative log-likelihood difference with respect to the minimum as a function of Δm_s.

8 Results for Δm_s

Assuming the values for the physics parameters given in Table 1, the variation in the data of the log-likelihood, as a function of the free parameter Δm_s, is shown in Fig. 6. The difference in log-likelihood is plotted relative to its global minimum and remains constant for Δm_s larger than 20 ps^{-1}. The global minimum occurs at $\Delta m_s = 15.9 \pm 1.6$(stat.) ps^{-1} but is not sufficiently deep to claim a measurement.

In order to extract a lower limit on Δm_s and to facilitate combination with other analyses, the results are also presented in terms of the "amplitude" fit. In this method [19] the magnitude of B$_s^0$ oscillations is measured at fixed values of the frequency Δm_s, using a modified likelihood function that depends on a new parameter, the B$_s^0$ oscillation amplitude $\mathcal{A}$. This is achieved by replacing the probability density function of the B$_s^0$ source given in Eq. (6) with

$$\frac{e^{-t_0/\tau_s}}{2\tau_s} \left[1 + \mu_0 \mathcal{A} \cos\left(\Delta m_s\, t_0\right)\right] . \tag{11}$$

For each value of Δm_s, the new negative log-likelihood is then minimized with respect to $\mathcal{A}$, leaving all other parameters (including Δm_s) fixed. The minimum is well behaved and very close to parabolic. At each value of Δm_s one can thus obtain a measurement of the amplitude with Gaussian error, $\mathcal{A} \pm \sigma_{\mathcal{A}}^{\text{stat}}$. If Δm_s is close to the true value, one expects $\mathcal{A} = 1$ within the estimated uncertainty; however, if Δm_s is far from its true value, a measurement consistent with $\mathcal{A} = 0$ is expected.

The amplitude fit results are displayed in Fig. 7 as a function of Δm_s. A peak in the amplitude, corresponding to the minimum observed in the negative log-likelihood, can be seen around $\Delta m_s = 16$ ps^{-1}. At this value, the measured amplitude is $2.2\,\sigma$ away from zero; as for the likelihood, this is not significant enough to claim a measurement of Δm_s.

A value of Δm_s can be excluded at 95% CL if $\mathcal{A} + 1.645\,\sigma_{\mathcal{A}} < 1$. Taking into account all systematic uncertainties described in the next section, all values of Δm_s below 9.5 ps^{-1}
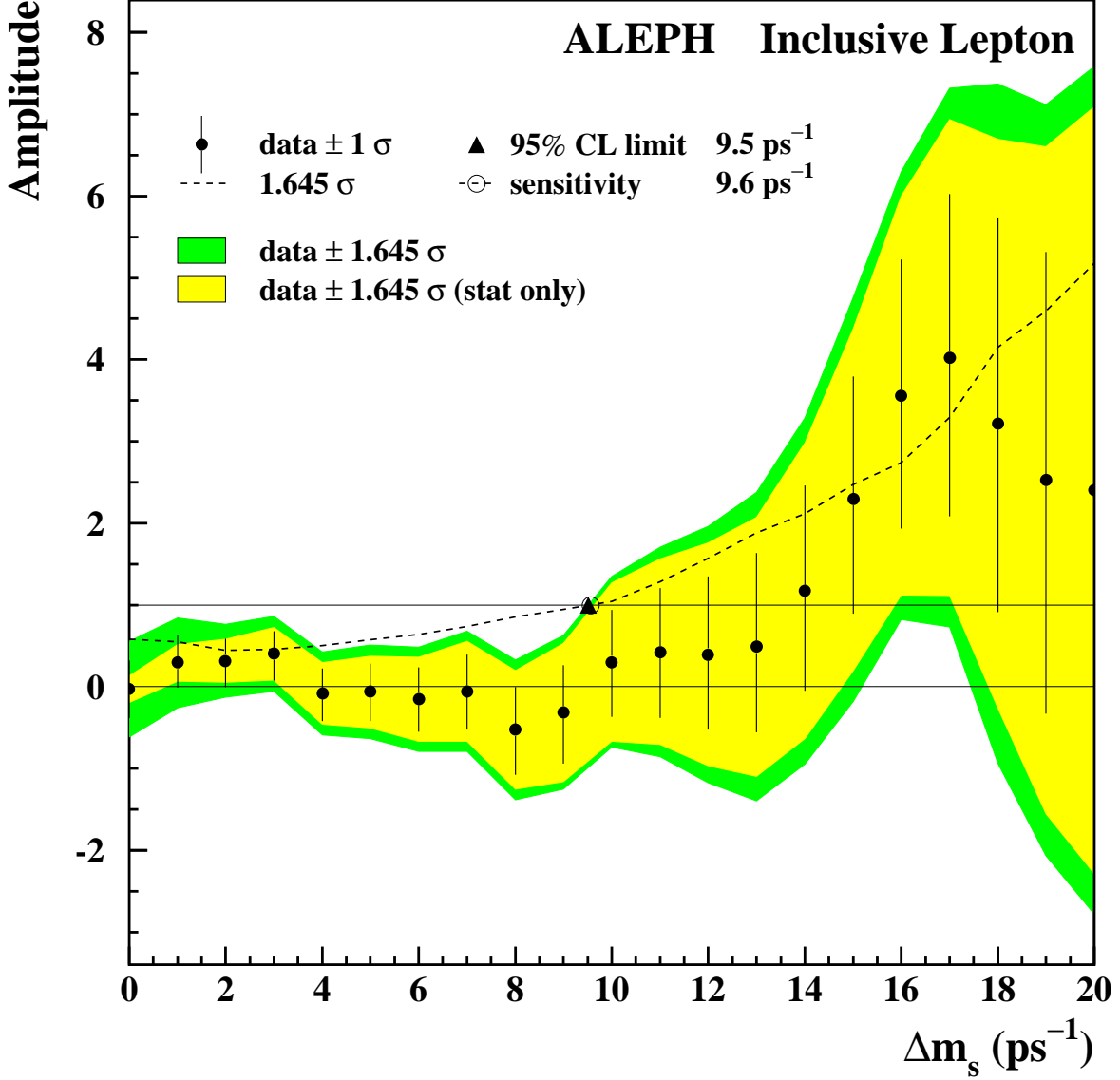
14

Figure 7: Measured B_s^0 oscillation amplitude as a function of Δm_s for this analysis. The error bars represent the 1σ total uncertainties, and the shaded bands show the one-sided 95% CL contour, with and without systematic effects included.

are excluded at 95% CL. The sensitivity, estimated from the data as the value of Δm_s at which $1.645\,\sigma_{\mathcal{A}} = 1$, is 9.6 ps^{-1}. Ignoring systematic uncertainties would increase the 95% CL lower limit and sensitivity by 0.1 ps^{-1} and 0.6 ps^{-1} respectively.

9   Systematic uncertainties

The systematic uncertainties on the B_s^0 oscillation amplitude $\sigma_{\mathcal{A}}^{\mathrm{syst}}$ are calculated, using the prescription of Ref. [19], as

$$\sigma_{\mathcal{A}}^{\mathrm{syst}} = \mathcal{A}^{\mathrm{new}} - \mathcal{A}^{\mathrm{nom}} + (1 - \mathcal{A}^{\mathrm{nom}})\frac{\sigma_{\mathcal{A}}^{\mathrm{new}} - \sigma_{\mathcal{A}}^{\mathrm{nom}}}{\sigma_{\mathcal{A}}^{\mathrm{nom}}} \tag{12}$$

where the superscript "nom" refers to the amplitude values and statistical uncerainties obtained using the nominal values for the various parameters and "new" refers to the new amplitude values obtained when a single parameter is changed and the analysis repeated (including a re-evaluation of the distributions of the discriminating variables used for the b-flavour tagging). The total systematic uncertainty is the quadratic sum of the following contributions.

- **Sample composition:** The systematic uncertainty on the sample composition is obtained by varying the assumed values for the b-hadron fractions $f_{B_s^0}$, $f_{b\text{-baryon}}$ and the various lepton sources (b $\to \ell$, b $\to$ c $\to \ell$, etc ...) by the uncertainties quoted in Table 1. The statistical uncertainty on the purities determined from Monte Carlo is also propagated.

  A comparison of data and Monte Carlo fractions for the different B_s^0 purity classes shows small deviations, the largest relative difference of 16% occurring in the first class of Table 3. The systematic uncertainty due to the B_s^0 purity classification procedure is evaluated by shifting, in each class, all five purities (B_s^0, B_d^0, ...) in the direction of their respective overall averages, $\overline{\alpha}_j$ given in Table 2, by a fraction $\gamma = \pm 20\%$ of their differences with respect to these averages:

  $$\alpha_{jkl} \to \alpha_{jkl} + \gamma(\alpha_{jkl} - \overline{\alpha}_j).\qquad(13)$$

  As this is performed coherently in all B_s^0 purity classes, the procedure is rather conservative and ensures that the overall average purities remain unchanged. Not using the B_s^0 purity classification would decrease the Δm_s statistical sensitivity by 0.7 ps^{-1}.

  For the fraction of charm and uds backgrounds a relative variation of $\pm 25\%$ is propagated, as suggested from a comparison between data and Monte Carlo performed in Ref. [20].

- **Proper time resolution:** For the systematic uncertainty on the proper time resolution, the correction factors presented in Tables 4 and 5 are varied by $\pm 1\sigma$. The scale factors ($S_l^{\text{dat}} = 1.02 \pm 0.03$ and $f_l^{\text{dat}} = 1.20 \pm 0.09$) for the decay length resolution, obtained from the lifetime fit to the data, are also varied by their measured uncertainty. In addition, a possible bias of ± 0.055 ps/cm is considered on the determination of the boost term; this value corresponds to the observed shift between the measured and simulated boost term distributions and represents approximately 1% of the average boost term. Finally the boost term resolution is given a relative variation of $\pm 10\%$ ($S_g^{\text{dat}} = 1.0 \pm 0.1$), which is conservative given the close agreement between the measured and simulated boost distributions.

- **b-quark fragmentation:** The average fraction of energy taken by a b-hadron during the fragmentation process, $\langle X_E \rangle = 0.702 \pm 0.008$, is varied by its measured uncertainty. The corresponding effects on the sample composition, mistags and resolutions are propagated.

- **Mistag:** Based on data/Monte Carlo comparisons of the tagging variables, performed for the D_s^--based analyses [1, 2], absolute variations of $\pm 0.8\%$ for the

16

first tagging class (opposite hemisphere charge) and $\pm 2\%$ for all other classes (fragmentation kaon and opposite lepton) are applied to the mistag rates. In addition, the $\pm 1\sigma$ statistical uncertainty from Monte Carlo is propagated.

The changes in mistag due to variation of the $b \to c \to \ell$ fraction are included as part of the sample composition systematic uncertainty.

- **Lifetimes, Δm_{d}, R_{b} and R_{c}:** The values assumed for the various b-hadron lifetimes, Δm_{d}, R_{b} and R_{c} are varied within the uncertainties quoted in Table 1.

- **Difference in decay width:** A possible decay width difference $\Delta\Gamma_{\mathrm{s}}/\Gamma_{\mathrm{s}}$ between the two mass eigenstates of the B_{s}^0 meson has been ignored in the likelihood fit. The fit is therefore repeated with a modified likelihood assuming $\Delta\Gamma_{\mathrm{s}}/\Gamma_{\mathrm{s}} = 0.27$, equal to the theoretical prediction of Ref. [21], $\Delta\Gamma_{\mathrm{s}}/\Gamma_{\mathrm{s}} = 0.16^{+0.11}_{-0.09}$, plus its quoted positive uncertainty.

- **Cascade bias:** In the likelihood expression of Eq. (8) each b-hadron component is treated using a single resolution function and mistag. No attempt is made to treat separately the $b \to \ell$ (direct) and $b \to c \to \ell$ (cascade) decays. While the former is characterized by a good proper time resolution and mistag, the latter has a degraded decay length resolution and a somewhat biased decay length because of the charm lifetime. In addition, the sign of the lepton is changed, leading to a different total mistag. To study the possible bias arising from the correlation between the poor decay length resolution and degraded tagging performance of the cascade events, two different fast Monte Carlo experiments are generated with a true value of Δm_{s} equal to 50 ps^{-1}. In the first the b-hadron decays are generated using the average mistag and resolution; in the second, the primary and cascade components are generated separately, each with their appropriate mistag and resolution. For both experiments, the corresponding amplitude plot is obtained using the likelihood described in Section 7, i.e. with average mistags and resolutions.

  The fast Monte Carlo experiment generated using the average b-hadron properties, yields an amplitude spectrum consistent with zero, as expected (since the fitting function is based on the same probability distributions as the fast Monte Carlo generator). In contrast, the experiment in which the direct and cascade decays are generated separately shows a small amplitude bias at low and very large Δm_{s}. Since the bias is small, especially in the region where the limit is set, and would cause the limit and sensitivity to be slightly underestimated, no attempt is made to correct for this effect; instead the deviations of the amplitude from zero observed are treated as a systematic uncertainty.

The relative importance of the various systematic uncertainties, as a function of Δm_{s}, is shown in Table 6. Except at low Δm_{s} the systematic uncertainties are generally small compared to the statistical uncertainty. At $\Delta m_{\mathrm{s}} = 10$ ps^{-1}, the most important contributions are from $f_{\mathrm{B}_{\mathrm{s}}^0}$ and the b-flavour tagging.

Table 6: Measurement of the B_s^0 oscillation amplitude, $\mathcal{A}$, for various oscillation frequencies together with the statistical uncertainty, $\sigma_{\mathcal{A}}^{\mathrm{stat}}$, and the total systematic uncertainty, $\sigma_{\mathcal{A}}^{\mathrm{syst}}$; a breakdown of $\sigma_{\mathcal{A}}^{\mathrm{syst}}$ in several categories of systematic effects is also given.

Δm_{s}	0 ps^{-1}	5 ps^{-1}	10 ps^{-1}	15 ps^{-1}
$\mathcal{A}$	-0.030	-0.065	0.303	2.291
$\sigma_{\mathcal{A}}^{\mathrm{stat}}$	± 0.099	± 0.267	± 0.590	± 1.271
$\sigma_{\mathcal{A}}^{\mathrm{syst}}$	$+0.340$ -0.340	$+0.223$ -0.235	$+0.232$ -0.324	$+0.801$ -0.582
Systematic contributions:				
$- R_{\mathrm{b}}, R_{\mathrm{c}}$	$+0.001$ -0.001	$+0.002$ -0.001	$+0.001$ -0.002	$+0.001$ -0.005
$- f_{\mathrm{B}_s^0} = \mathcal{B}(\bar{\mathrm{b}} \to \mathrm{B}_s^0)$	$+0.046$ -0.035	$+0.146$ -0.112	$+0.133$ -0.109	$+0.217$ -0.173
$- f_{\mathrm{b\text{-}baryon}} = \mathcal{B}(\mathrm{b} \to \mathrm{b\text{-}baryon})$	$+0.008$ -0.010	$+0.026$ -0.018	$+0.028$ -0.023	$+0.007$ -0.002
$-$ charm fraction	$+0.012$ -0.012	$+0.019$ -0.016	$+0.021$ -0.018	$+0.051$ -0.043
$-$ uds fraction	$+0.008$ -0.008	$+0.023$ -0.026	$+0.032$ -0.038	$+0.078$ -0.091
$- \mathrm{b} \to \ell, \mathrm{b} \to \mathrm{c} \to \ell, \mathrm{b} \to \bar{\mathrm{c}} \to \ell, \mathrm{c} \to \ell$	$+0.065$ -0.013	$+0.000$ -0.055	$+0.000$ -0.121	$+0.464$ -0.000
$-$ purities (MC stat.)	$+0.047$ -0.041	$+0.078$ -0.070	$+0.076$ -0.075	$+0.104$ -0.108
$- \mathrm{B}_s^0$ purity classes	$+0.017$ -0.009	$+0.000$ -0.007	$+0.010$ -0.018	$+0.140$ -0.187
$- \Delta m_{\mathrm{d}}$	$+0.037$ -0.037	$+0.002$ -0.002	$+0.001$ -0.001	$+0.000$ -0.003
$-$ b-hadron lifetimes	$+0.033$ -0.000	$+0.000$ -0.046	$+0.027$ -0.037	$+0.282$ -0.000
$-$ decay length resolution	$+0.000$ -0.000	$+0.025$ -0.025	$+0.054$ -0.057	$+0.050$ -0.021
$-$ boost term resolution	$+0.010$ -0.010	$+0.030$ -0.033	$+0.048$ -0.059	$+0.205$ -0.191
$-$ b-fragmentation	$+0.023$ -0.000	$+0.012$ -0.070	$+0.067$ -0.085	$+0.509$ -0.403
$-$ b-flavour tagging	$+0.317$ -0.332	$+0.138$ -0.132	$+0.132$ -0.207	$+0.233$ -0.219
$- \Delta\Gamma_{\mathrm{s}}/\Gamma_{\mathrm{s}}$	$+0.000$ -0.002	$+0.012$ -0.000	$+0.011$ -0.000	$+0.018$ -0.000
$-$ cascade bias	$+0.060$ -0.000	$+0.000$ -0.087	$+0.000$ -0.085	$+0.000$ -0.069

10 Checks

Using a fast Monte Carlo generator which takes into account all details of the sample composition, the resolution functions, the mistag rates and the distributions of x^{eff}, the average amplitude over many fast Monte Carlo experiments is found to be consistent with unity for $\Delta m_{\mathrm{s}} = \Delta m_{\mathrm{s}}^{\mathrm{true}}$ and with zero for any value of Δm_{s} if $\Delta m_{\mathrm{s}}^{\mathrm{true}} = \infty$. The estimate, $\sigma_{\mathcal{A}}^{\mathrm{stat}}$, of the statistical uncertainty on the amplitude has also been verified by studying the distribution of $\mathcal{A}/\sigma_{\mathcal{A}}^{\mathrm{stat}}$ for cases where $\mathcal{A} = 0$ is expected. The mean value and RMS of such a distribution obtained with fast Monte Carlo experiments generated with $\Delta m_{\mathrm{s}}^{\mathrm{true}} = \infty$ are found to be consistent with 0 and 1.

A likelihood fit for Δm_{s} performed on a $Z \to q\bar{q}$ Monte Carlo sample having the same statistics as the data and generated with a true value of Δm_{s} of 3.33 ps^{-1} yields
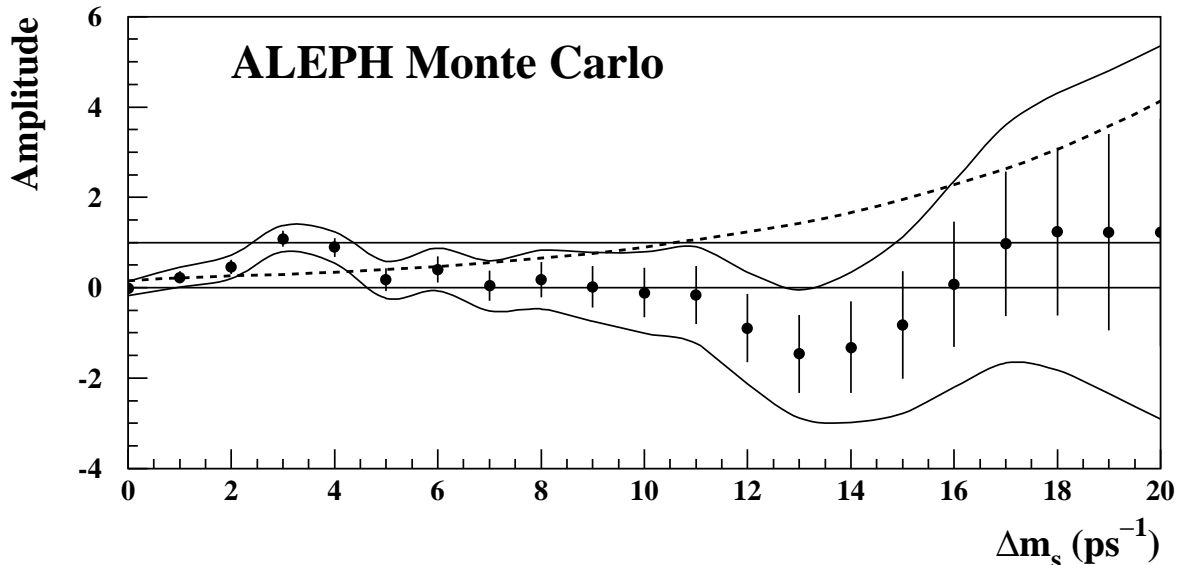
Figure 8: Measured B_s^0 oscillation amplitude as a function of Δm_s in the $Z \to q\bar{q}$ Monte Carlo. The error bars represent the 1σ statistical uncertainties, the solid curve the one-sided 95% CL contour (systematic effects not included). The dotted line is $1.645\,\sigma$. The generated value of Δm_s is 3.33 ps^{-1}.

$\Delta m_s = 3.31 \pm 0.12$(stat.) ps^{-1}, in agreement with the input value. Performing an amplitude fit on the same Monte Carlo events yields the results shown in Fig. 8. As expected, the amplitude is consistent with 1 at the true value of Δm_s. The sensitivity estimated from this Monte Carlo sample (ignoring systematic uncertainties) is 10.6 ps^{-1}, a little higher than that obtained from the data, 10.2 ps^{-1}, due to the slightly better decay length resolution in Monte Carlo.

As a further check of the assumed mistags and sample composition, the analysis is used to measure Δm_d in the data. Fixing Δm_s to 50 ps^{-1} and minimizing the negative log-likelihood with respect to Δm_d gives $\Delta m_d = 0.451 \pm 0.024$(stat.) ps^{-1}, consistent with the latest world average of 0.463 ± 0.018 ps^{-1} [13]. Figure 9 shows that the fitted B_d^0 oscillation amplitude is consistent with that observed in the $Z \to q\bar{q}$ Monte Carlo and has the expected value of 1 at the minimum of the negative log-likelihood. To check that the sample composition and mistags assumed for each B_s^0 purity class and tagging class are reasonable, a fit for the B_d^0 oscillation amplitude is performed separately in each class. At $\Delta m_d = 0.451$ ps^{-1} a value of $\mathcal{A}$ consistent with 1 is found in all classes; the largest deviation being $1.5\,\sigma_{\text{stat}}$ in the last B_s^0 purity class ("remainder").

11 Combination with D_s^- analyses

The amplitudes measured in this analysis and in the two ALEPH D_s^- analyses [1, 2] are combined. The small number of events common to both this analysis and the D_s^-– lepton analysis are removed from the inclusive lepton sample before combining the results. The following sources of systematic uncertainty are treated as fully correlated: the values assumed for $f_{B_s^0}$, $f_{\text{b-baryon}}$, Δm_d and the various b-hadron lifetimes, the b fragmentation,
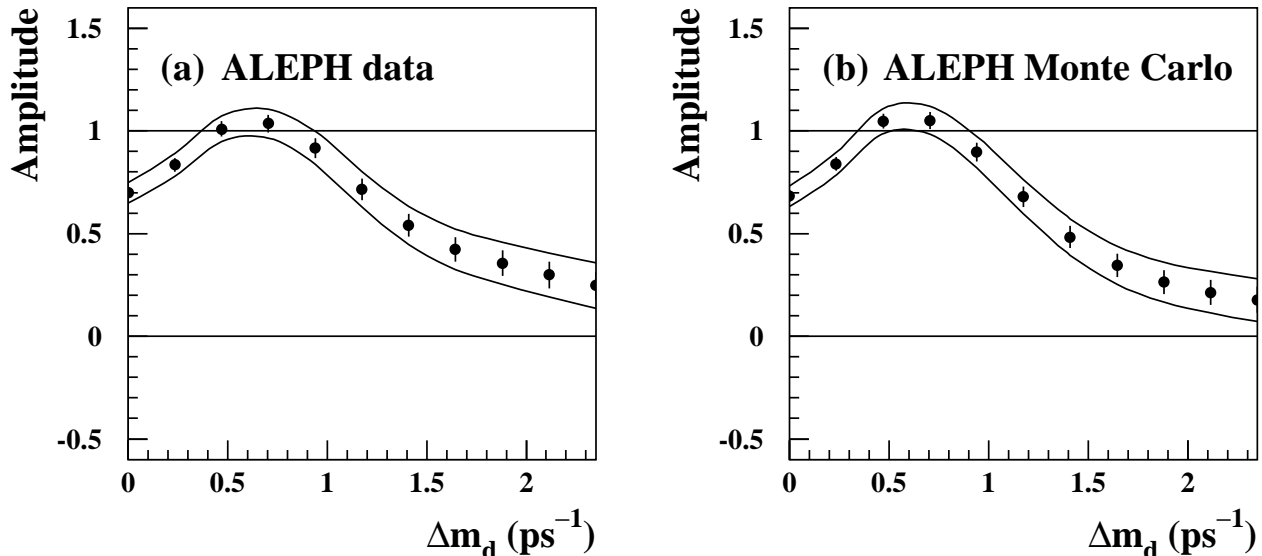
19

Figure 9: Measured B_d^0 oscillation amplitude as a function of Δm_d in (a) the data and (b) the $Z \to q\bar{q}$ Monte Carlo. The error bars represent the 1σ total uncertainties and the curves the one-sided 95% CL contour (systematic effects not included).

Table 7: Combined measurements of the B_s^0 oscillation amplitude $\mathcal{A}$ as a function of Δm_s (in ps^{-1}), together with the statistical uncertainty $\sigma_{\mathcal{A}}^{\text{stat}}$ and the total systematic uncertainty $\sigma_{\mathcal{A}}^{\text{syst}}$.

Δm_s	$\mathcal{A} \pm \sigma_{\mathcal{A}}^{\text{stat}} \pm \sigma_{\mathcal{A}}^{\text{syst}}$	Δm_s	$\mathcal{A} \pm \sigma_{\mathcal{A}}^{\text{stat}} \pm \sigma_{\mathcal{A}}^{\text{syst}}$	Δm_s	$\mathcal{A} \pm \sigma_{\mathcal{A}}^{\text{stat}} \pm \sigma_{\mathcal{A}}^{\text{syst}}$
0.00	$+0.03 \pm 0.08 \pm 0.18$	7.00	$-0.15 \pm 0.30 \pm 0.18$	14.00	$+1.21 \pm 0.86 \pm 0.47$
1.00	$+0.16 \pm 0.11 \pm 0.18$	8.00	$-0.24 \pm 0.35 \pm 0.21$	15.00	$+1.98 \pm 0.99 \pm 0.54$
2.00	$-0.13 \pm 0.13 \pm 0.17$	9.00	$-0.05 \pm 0.40 \pm 0.23$	16.00	$+2.76 \pm 1.16 \pm 0.57$
3.00	$+0.13 \pm 0.16 \pm 0.19$	10.00	$+0.30 \pm 0.46 \pm 0.27$	17.00	$+2.86 \pm 1.37 \pm 0.61$
4.00	$+0.00 \pm 0.18 \pm 0.16$	11.00	$+0.37 \pm 0.54 \pm 0.37$	18.00	$+2.22 \pm 1.61 \pm 0.77$
5.00	$-0.10 \pm 0.22 \pm 0.18$	12.00	$+0.47 \pm 0.64 \pm 0.39$	19.00	$+1.85 \pm 1.88 \pm 0.98$
6.00	$-0.20 \pm 0.25 \pm 0.17$	13.00	$+0.65 \pm 0.75 \pm 0.42$	20.00	$+2.02 \pm 2.19 \pm 1.29$

the decay length resolution bias in the Monte Carlo simulation S_l^{dat} and f_l^{dat}, the mistag probabilities, and the use of the effective discriminating variable. Since the physics parameters assumed in the three analyses are slightly different, the D_s^- results are adjusted to the more recent set of physics parameters listed in Table 1 before averaging. The combined amplitude plot is displayed in Fig. 10 and the corresponding numerical values are listed in Table 7. All values of Δm_s below 9.6 ps^{-1} are excluded at 95% CL. The combined sensitivity is 10.6 ps^{-1}.

As the statistical correlation between this analysis and the previous ALEPH dilepton and lepton-kaon analyses [3, 5] is very large, no significant improvement in sensitivity is expected if these latter analyses were included in the combination.
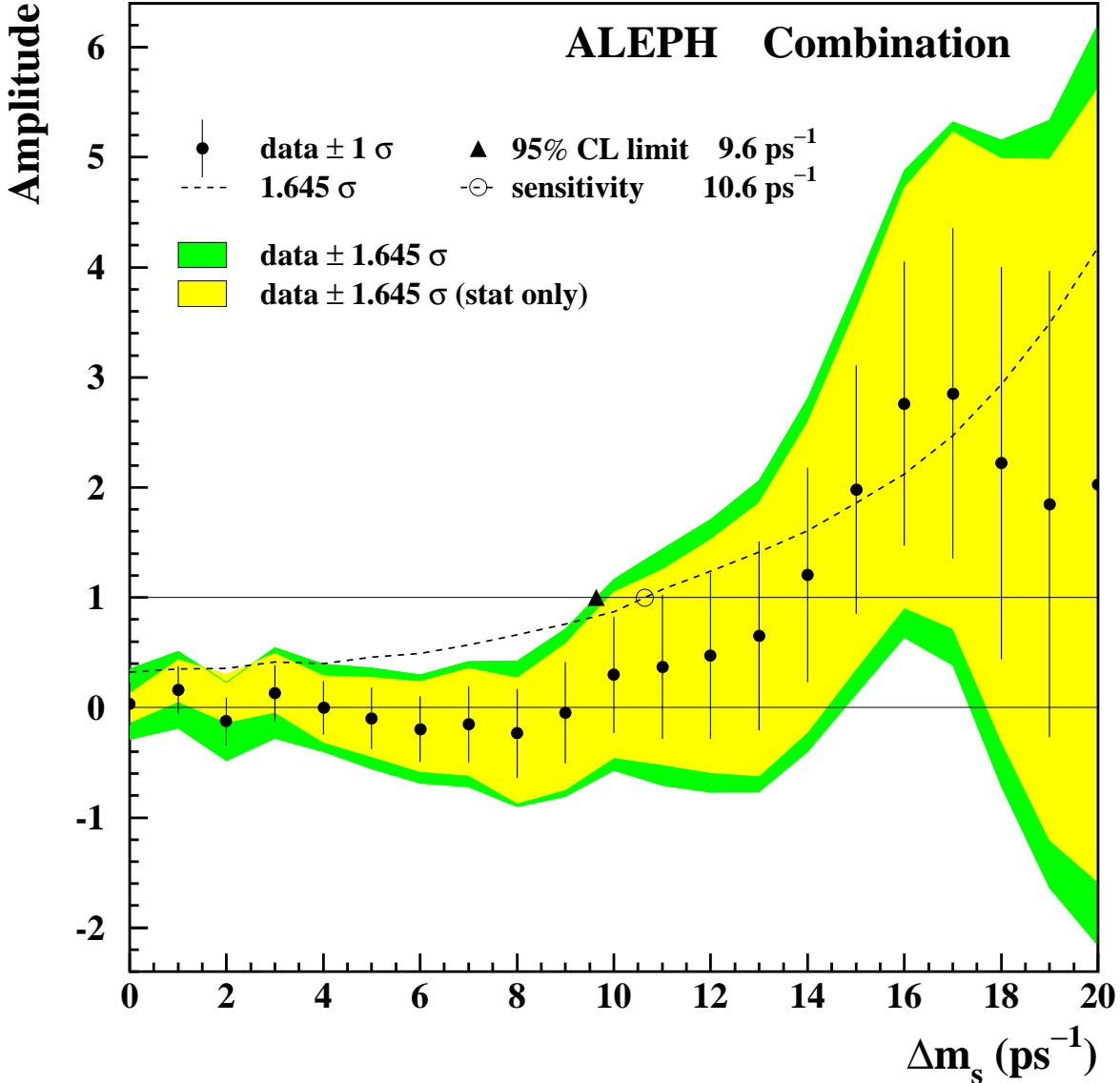
Figure 10: Measured B_s^0 oscillation amplitude as a function of Δm_s for the combination of this analysis with the ALEPH D_s^- based analyses.

12 Conclusion

From a sample of 33023 inclusive lepton events, all values of Δm_s below 9.5 ps^{-1} are excluded at 95% CL using the amplitude method. This analysis supersedes the previous ALEPH inclusive lepton analysis [4] and provides the highest sensitivity and highest 95% CL lower limit on Δm_s of any B_s^0 mixing analysis published to date [1, 2, 3, 4, 22, 23].

Taking into account correlated systematic uncertainties the combination with the ALEPH D_s^- based analyses yields $\Delta m_s > 9.6$ ps^{-1} at 95% CL.

Acknowledgements

It is a pleasure to thank our colleagues in the accelerator divisions of CERN for the excellent performance of LEP. Thanks are also due to the technical personnel of the collaborating institutions for their support in constructing and maintaining the ALEPH experiment. Those of us not from member states wish to thank CERN for its hospitality.

References

[1] ALEPH Collaboration, *"Study of the $B_s^0 - \bar{B}_s^0$ oscillation frequency using $D_s^- - \ell^+$ combinations in Z decays"*, Phys. Lett. B **377** (1996) 205.

[2] ALEPH Collaboration, *"Study of B_s^0 oscillations and lifetime using fully reconstructed D_s^- decays"*, Eur. Phys. J. C 4 (1998) 367.

[3] ALEPH Collaboration, *"An investigation of B_d^0 and B_s^0 oscillation"*, Phys. Lett. B **322** (1994) 441.

[4] ALEPH Collaboration, *"Limit on B_s^0 oscillation using a jet charge method"*, Phys. Lett. B **356** (1995) 409.

[5] ALEPH Collaboration, *"Combined limit on the B_s^0 oscillation frequency"*, contribution PA08–020 to the 28$^\text{th}$ International Conference on High Energy Physics, Warsaw, Poland, July 1996.

[6] ALEPH Collaboration, *"ALEPH: a detector for electron-positron annihilations at LEP"*, Nucl. Instrum. Methods A **294** (1990) 121, erratum **303** (1991) 393;
B. Mours et al., Nucl. Instrum. Methods A **379** (1996) 101.

[7] ALEPH Collaboration, *"Performance of the ALEPH detector at LEP"*, Nucl. Instrum. Methods A **360** (1995) 481.

[8] ALEPH Collaboration, *"Improved measurements of electroweak parameters from Z decays into fermion pairs"*, Z. Phys. C **53** (1992) 1.

[9] T. Sjöstrand and M. Bengtsson, Computer Phys. Commun. **43** (1987) 367.

[10] ALEPH Collaboration, *"Heavy quark tagging with leptons in the ALEPH detector"*, Nucl. Instrum. Methods A **346** (1994) 461.

[11] JADE Collaboration, *"Experimental investigation of the energy dependence of the strong coupling strength"*, Phys. Lett. B **213** (1988) 235.

[12] ALEPH Collaboration, *"A precise measurement of $\Gamma(Z \to b\bar{b})/\Gamma(Z \to hadrons)$"*, Phys. Lett. B **313** (1993) 535.

[13] O. Schneider, *"Heavy quark spectroscopy, lifetimes and oscillations""*, CERN–PPE/97–143, to appear in the proceedings of the 18$^\text{th}$ International Symposium on Lepton-Photon Interactions, Hamburg, Germany, July 1997.

[14] The LEP Collaborations ALEPH, DELPHI, L3, OPAL, the LEP Electroweak Working Group and the SLD Heavy Flavour Group, *"A Combination of Preliminary Electroweak Measurements and Constraints on the Standard Model"*, CERN-PPE/97-154.

[15] ALEPH, DELPHI, L3, OPAL Collaborations, *"Combining heavy flavour electroweak measurements at LEP"*, Nucl. Instrum. Methods A **378** (1996) 101.

[16] ALEPH Collaboration, *"Measurement of mean lifetime and branching fractions of b-hadrons decaying to J/ψ"*, Phys. Lett. B **295** (1992) 396.

[17] ALEPH Collaboration, *"Measurement of the B_s^0 lifetime"*, Phys. Lett. B **322** (1994) 275.

[18] O. Leroy, *"Etude du mélange $B_s^0 - \bar{B}_s^0$ dans l'expérience ALEPH au LEP"*, Ph.D. thesis, CPPM-T-1998-01, Université de la Méditerranée, 1998.

[19] H.-G. Moser and A. Roussarie, Nucl. Instrum. Methods A **384** (1997) 491.

[20] ALEPH Collaboration, *"Measurement of the b forward-backward asymmetry and mixing using high-$p_\perp$ leptons"*, Phys. lett. B **384** (1996) 414.

[21] M. Beneke, G. Buchalla and I. Dunietz, Phys. Rev. D **54** (1996) 4419.

[22] DELPHI Collaboration, *"Search for $B_s^0 - \bar{B}_s^0$ oscillations"*, Phys. Lett. B **414** (1997) 382.

[23] OPAL Collaboration, *"An updated study of B meson oscillations using dilepton events"*, Z. Phys. C **76** (1997) 417; *"A study of B meson oscillations using hadronic Z decays containing leptons"*, Z. Phys. C **76** (1997) 401.